Appl Phys A (2011) 103: 403–411
DOI 10.1007/s00339-011-6353-9

Applied Physics A
Materials Science & Processing

Fabrication of double- and multi-walled carbon nanotube transparent conductive films by filtration-transfer process and their property improvement by acid treatment

Guang-Hui Xu · Jia-Qi Huang · Qiang Zhang · Meng-Qiang Zhao · Fei Wei

Received: 6 December 2010 / Accepted: 17 February 2011 / Published online: 16 March 2011

Abstract Double-walled carbon nanotubes (DWCNTs) and two kinds of vertically aligned multi-walled carbon nanotubes were employed as raw materials to fabricate transparent conductive films (TCFs). DWCNTs constructed the densest conductive network at the same transmittance, and the corresponding TCFs showed the best performance (320 Ω/□ at 75.0% T). The ratio of dc conductivity to optical conductivity (σ_{dc}/σ_{op}) of the as-dispersed DWCNTs was 3.88. The as-obtained TCFs were dipped in HNO_3 solution to improve their performances. Attributed to the removal of sodium dodecyl sulfate molecules, reduction of film thickness, and doping with electron acceptors (such as oxygen), the surface resistance after HNO_3 treatment decreased. The σ_{dc}/σ_{op} ratio of the DWCNTs was further increased to 5.24.

1 Introduction

Transparent conducting films (TCFs), which were fabricated from inorganic (indium tin oxide (ITO), fluorine-doped tin oxide, doped zinc oxide, etc.) or organic materials (such as carbon nanotube (CNT) networks, graphene, and conductive polymers), can act both as an ohmic contact for carrier transport out of the photovoltaic material and a window for light to pass through to the active material beneath (where carrier generation occurs) [1–4]. Up to now, TCFs are essential elements of flat-panel displays [5, 6], organic light-emitting diodes [1], solar cells [4], and electrochromic devices [3]. Recently, the fabrication of TCFs with CNTs [7–17] and other nanostructured carbon (such as graphene) [18–20] as the raw materials was highly concerned. TCFs based on CNTs and graphene possess high optical transparency and electrical conductivity, which now have matched the demand for certain applications such as touch screens (500 Ω/□ at 85% T is needed for practical applications). Compared with ITO, which is the most widely used material for TCFs, CNTs are far more flexible and environmentally resistant [9, 19, 21]. In addition, carbon is a much more abundant resource than indium.

Up to now, single-walled CNTs (SWCNTs) were widely selected as raw CNTs to fabricate TCFs. The arc-discharge SWCNTs showed good performance to obtain TCFs with high conductivity at the same transparency [22]. Recently, it was reported that TCFs from double-walled CNTs (DWCNTs) or multi-walled CNTs (MWCNTs) illustrated better performance than those made of SWCNTs [14, 23–25].

The available SWCNTs were always a mixture of semiconductive and metallic CNTs. Density differentiation sorted metallic SWCNT films showed a lower surface resistance than unsorted SWCNT films [10]. SWCNTs usually became short after purification and dispersion, with a length of <1 μm [14, 26, 27]. Recently, Kaskela et al. demonstrated an aerosol chemical vapor deposition (CVD) process to dry deposit large-area SWCNT networks in which the bundle length was about 10 μm, and reached a performance

G.-H. Xu · J.-Q. Huang · Q. Zhang · M.-Q. Zhao · F. Wei (✉)
Beijing Key Laboratory of Green Chemical Reaction Engineering and Technology, Department of Chemical Engineering, Tsinghua University, Beijing 100084, China
e-mail: wf-dce@tsinghua.edu.cn
Fax: +86-10-62772051

G.-H. Xu
e-mail: xgh06@mails.tsinghua.edu.cn

J.-Q. Huang
e-mail: hjq03@mails.tsinghua.edu.cn

Q. Zhang
e-mail: zhang-qiang@mails.tsinghua.edu.cn

M.-Q. Zhao
e-mail: zhaomq08@gmail.com

of 110 Ω/□ at 90% T after chemical doping [28]. Thus, it is quite important to preserve the long length and large aspect ratio of CNTs. Actually, pure and perfect long metallic SWCNTs are the ideal raw materials for CNT TCFs. Practically, due to problems in synthesis and purification, such SWCNTs are difficult to obtain in large scale. However, most MWCNTs exhibit a metallic conductive behavior, and MWCNTs with a length of 1–8 mm can be easily obtained in array form [29–31]. The aligned CNTs are good precursors to be dispersed into long individual CNTs. Recently, vertically aligned CNT (VACNT) arrays, in which the CNTs with large aspect ratio are well oriented, can be easily produced by radial growth on spheres or intercalated growth among lamellar catalysts [32, 33]. A 3.0 kg/h productivity of VACNT arrays at a low cost has been achieved in a fluidized bed reactor [34]. Recently, density differentiation sorted DWCNT films after $SOCl_2$ doping showed a low surface resistance [14]. In addition, DWCNTs exhibit a high structural stability in comparison with that of SWCNTs. DWCNTs with high quality can also be produced in a fluidized bed at a large scale [35]. This provides a possibility to explore the application of industrial aligned MWCNTs and DWCNTs for TCFs.

In this contribution, both long DWCNTs and vertically aligned MWCNTs, which can be mass produced at an industrial scale at a low cost, were selected as raw materials to fabricate D/MWCNT-based TCFs. The properties of the as-obtained TCFs were further enhanced by acid treatment to meet applications for touch screens.

2 Experimental section

2.1 Materials

VACNT arrays fabricated by a floating catalyst chemical vapor deposition (CVD) [32] and a thermal CVD method [36] were used, and they were named as VACNT array-1 and VACNT array-2, respectively. As shown in Table 1, the CNTs in VACNT array-1 were of length 5.0 mm and a diameter distribution of 46.9 ± 25.2 nm, while the CNTs in VACNT array-2 were of length 0.2 mm and a diameter distribution of 11.0 ± 0.93 nm. Both VACNT arrays were directly used without any specific purification. DWCNTs were synthesized in a fluidized bed reactor by cracking CH_4 on a Fe/MgO catalyst and had a diameter distribution of 2.05 ± 0.93 nm [35]. The as-prepared powder was purified by sonication in HCl solution for 2 h to remove the residual catalyst.

2.2 Dispersion of CNTs

VACNT array-1 was firstly sheared into fluffy CNTs by high-speed shearing in air [29] and then dispersed in benzyl alcohol [37]. About 1.0 g of the VACNT array-1 was placed in a high-speed shearer with a rotor rotating at a speed of 24000 rpm for 60–600 s. The as-obtained fluffy CNTs were further dispersed in benzyl alcohol with a concentration of 4.0 mg/L. The suspension was stirred in the disintegrator for 10 min at a rotation speed of 6000 rpm.

For VACNT array-2, liquid shearing was directly applied. A CNT suspension with a concentration of 0.25 mg/L was stirred in the disintegrator for 30 min at a rotation speed of 6000 rpm.

The purified DWCNTs were dispersed by sonication with the assistance of sodium dodecyl sulfate (SDS). About 0.3 g of DWCNTs was added in ~500 mL of 1.0 wt.% SDS aqueous solution and sonicated by a sonication tip (20 kHz, 100 W) for 3 h. After the process, only part of DWCNTs was dispersed into small CNT bundles in the solvent and there were still big agglomerates in the dispersion. The dispersion was centrifuged at 5000 rpm for 10 min to precipitate the agglomerates. Then the upper 50% of the supernatant solution was carefully decanted for use, which was a solution of well-dispersed small CNT bundles.

2.3 Fabrication of TCFs

The TCFs were fabricated by a filtration method [38]. The dispersions of all kinds of CNTs were filtrated through a mixed cellulose ester (MCE) filter membrane (220-nm pore size), since it can be easily dissolved by acetone. The surface resistance of the film was controlled by filtrating a controlled volume of the dispersion. The deposited CNT films were then pressed against a polyethylene terephthalate (PET) substrate together with the MCE membrane and dried at 75°C in vacuum overnight under a 27-kPa load to improve adhesion between the CNTs and the PET substrate. Then the membrane on the PET substrate was placed directly in an acetone bath for 30 min to dissolve the MCE membrane, and then picked up and transferred to another clean acetone bath for 30 min to remove dissolved MCE diffused into the porous film in the first bath. The process was repeated (usually four times) to ensure the complete removal of the MCE. The final bath is typically a methanol bath. The films were picked up and dried to realize the transfer of the CNT film from the MCE membrane to the PET substrate.

2.4 HNO_3 treatment

The DWCNT TCFs were dipped in HNO_3 (65 wt.%) for 10–180 min. Then the film was picked up and dried at 80°C in an oven for 30 min. The TCF after 180-min treatment was further washed by de-ionized water several times. Silver paint was painted on the PET substrate until the resistance of the silver paint did not change much. The TCFs made from both CNT arrays were dipped in HNO_3 for 180 min and dried at 80°C for 30 min following the same procedure.

2.5 Characterization

The raw materials of different kinds of CNTs and the TCFs made from them were characterized by both scanning electron microscopy (SEM, JSM 7401F) and transmission electron microscopy (TEM, JEM 2010). The raw materials and TCFs were directly observed under SEM. Some drops from the diluted suspension were dropped onto a copper grid, dried in an oven (80°C), and then observed by TEM. For the DWCNT TCFs, the TCF on the MCE filter membrane was dipped in an acetone bath and the CNT film was picked up by the PET film with a TEM grid on it. The film was carefully washed in several acetone baths and a final methanol bath to remove the MCE completely. The optical properties of TCFs (without PET substrate) were measured by an A-722 grating spectrophotometer at a wavelength of 550 nm. Raman experiments were performed with a Raman spectrophotometer (Renishaw, RM2000) in ambient conditions. The spectra were recorded using a He–Ne laser excitation line of 633 nm. The dispersions of all kinds of CNTs were filtrated through MCE filter membranes, washed with de-ionized water, and dried at 75°C. Then the MCE membrane was dissolved in several acetone baths and a final methanol bath as described above. Opaque thick CNT films were picked up by glass slides and dried to get the samples for the Raman test. The surface resistance of TCFs and opaque DWCNT films treated by HNO_3 were obtained by a four-probe method.

3 Results and discussion

The SEM and TEM images of CNTs used for TCF fabrication in this contribution are shown in Fig. 1. Both the CNTs in VACNT array-1 and VACNT array-2 showed good alignment, and were perpendicular to the substrates (Figs. 1a and 1c). The DWCNTs after purification had a high purity and their bundle structure was clearly visualized (Fig. 1e). Compared with the MWCNT arrays, the graphene layers of DWCNTs had fewer defects (Fig. 1f).

Here, a filtration method was employed to fabricate CNT TCFs [38]. A typical photograph of a TCF on a PET substrate with a transmittance of over 80% is shown in Fig. 2a. The semi-transparent gray circle was a CNT film, which was homogeneously coated on the transparent PET substrate. As shown in Fig. 2b, the performances were 10.3 kΩ/□ at 74.4% T, 2.5 kΩ/□ at 79.7% T, and 0.32 kΩ/□ at 75.0% T for TCFs from VACNT array-1, VACNT array-2, and DWCNTs, respectively. The SEM images of TCFs made from different kinds of raw CNTs at the transmittance of 80% are shown in Figs. 2c–2e. VACNT array-1 was individually dispersed by the two-step shearing method [37] and had a length of tens of micrometers (Fig. 2c). VACNT array-2 was also well dispersed (Fig. 2d). Moreover, the conductive network was denser than that from VACNT array-1. DWCNTs were clustered into bundles and formed a very dense network. The sheet resistance of the TCF can be modeled by the sum of the series resistances of the CNTs and the number of cross junctions formed among the CNTs. The conductivity of the film is dominated by inter-tube hoping electron transport. The electrons transport via the hoping mechanism through these junctions [39]. The densest DWCNT networks had the greatest number of CNTs and junctions, and therefore the highest conductivity.

The length distribution of each kind of CNT after dispersion is shown in Fig. 2f. The average length and standard deviation of dispersed CNTs from VACNT array-1 and VACNT array-2 were 38.5 ± 19.3 and 13.8 ± 6.6 μm, respectively. The average length and standard deviation of DWCNT bundles after dispersion was 1.57 ± 0.61 μm. The aspect ratios were ∼820, ∼1250, and ∼760 for dispersed CNTs from VACNT array-1, VACNT array-2, and DWCNTs, respectively. The performances of D/MWCNT TCFs reported in this work were compared with the results in the literature (Fig. 3a) [6, 14, 19, 23, 24, 40–46]. The performances of TCFs made from VACNT array-2 and DWCNTs were superior to most reported results of MWCNT and DWCNT TCFs from the literature, respectively. The order of CNT lengths was VACNT array-1 > VACNT array-2 > DWCNTs. However, the order of TCF performances was DWCNTs > VACNT array-2 > VACNT array-1. MWCNTs in VACNT array-1 consisted of more graphene walls than those in VACNT array-2, and MWCNTs in VACNT array-2 consisted of more graphene walls than DWCNTs. MWCNTs suffered from deteriorated transmittance by absorption and Rayleigh scattering due to their large diameter [47].

To describe the performance of the TCFs more clearly, the electro-optical property for a metallic thin film (film thickness much smaller than wavelength of light) in air was used, which was similar to many reports for SWCNT TCFs [48, 49]. It can be expressed as follows:

$$T = \left(1 + \frac{Z_0}{2R_S}\frac{\sigma_{op}}{\sigma_{dc}}\right)^{-2}, \quad (1)$$

where R_S is the sheet resistance, T is the wavelength-dependent transmittance, σ_{dc} is the direct current (dc) conductivity, σ_{op} is the optical conductivity, and Z_0 is the characteristic impedance of free space (∼376.73 Ω). A material with relatively high conductivity and yet low optical absorbance as manifested by a large ratio of dc to optical conductivities, σ_{dc}/σ_{op}, is strongly desired for thin, transparent, conductive films for electrode applications in devices from liquid-crystal displays to organic light-emitting diodes and solar cells. Here, the thickness for a MWCNT film is approx. 50–100 nm, which cannot meet the assumption that the film thickness was much smaller than the wavelength of

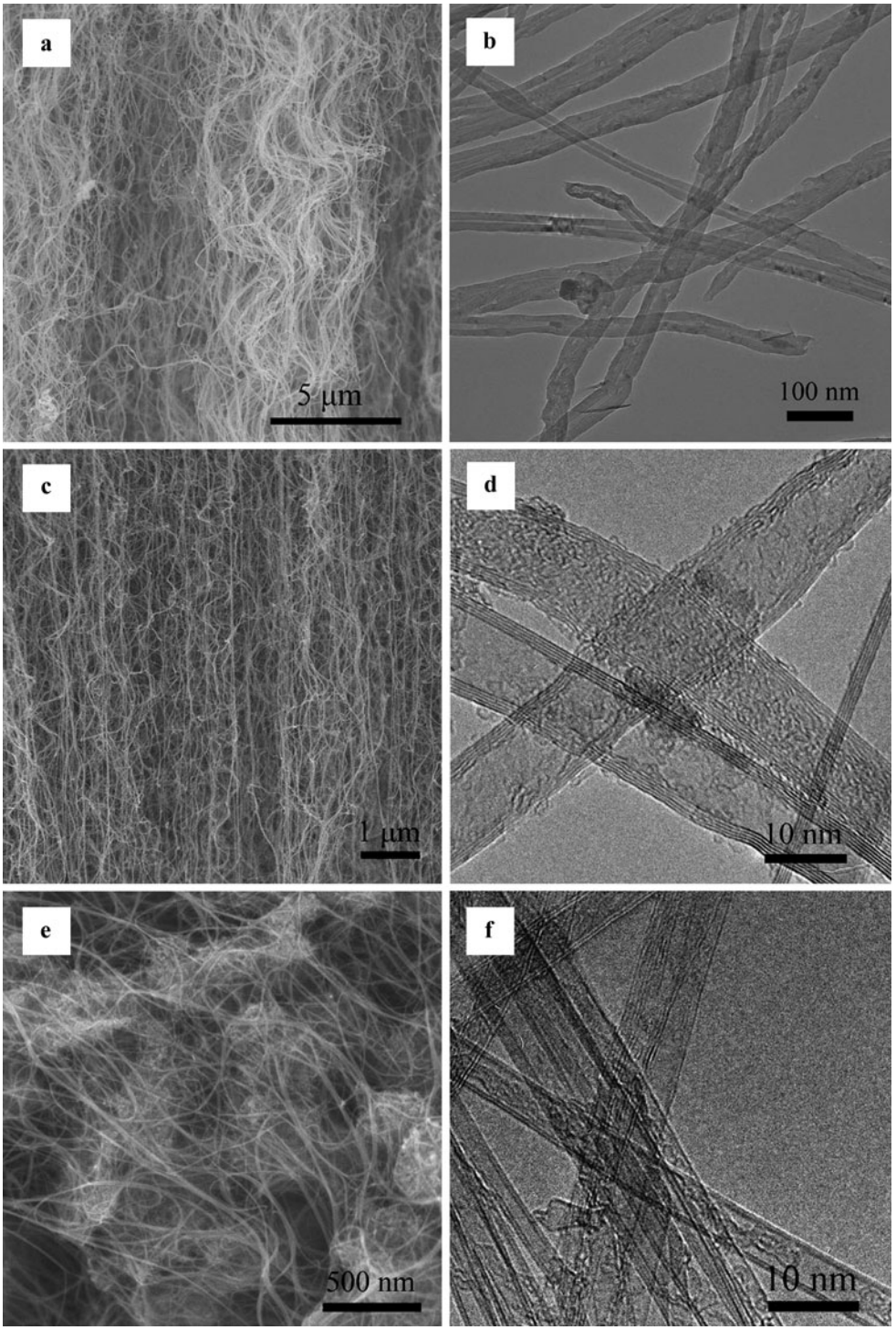

Fig. 1 SEM and TEM images of (**a**, **b**) VACNT array-1, (**c**, **d**) VACNT array-2, and (**e**, **f**) DWCNTs, respectively

light (550 nm). Thus, the modified equation by Geng et al. [45] as follows was used:

$$T = t\left(1 + \frac{Z_0}{2R_S}\frac{\sigma_{op}}{\sigma_{dc}}\right)^{-2}, \quad (2)$$

where t presents the diameter effect of the MWCNT film. The fitting curves are shown in Fig. 3b, which fitted well with the experimental data, and the fitting parameters are shown in Table 1.

For VACNT array-1 (diameter of 46.9 ± 25.2 nm), the σ_{dc}/σ_{op} ratio was just 0.139. For VACNT array-2, the diameter of the CNTs was small (11.0 ± 0.93 nm), and the σ_{dc}/σ_{op} ratio dispersed by the shearing method was 0.760. The σ_{dc}/σ_{op} ratio of DWCNTs (diameter of 2.05 ± 0.93 nm)

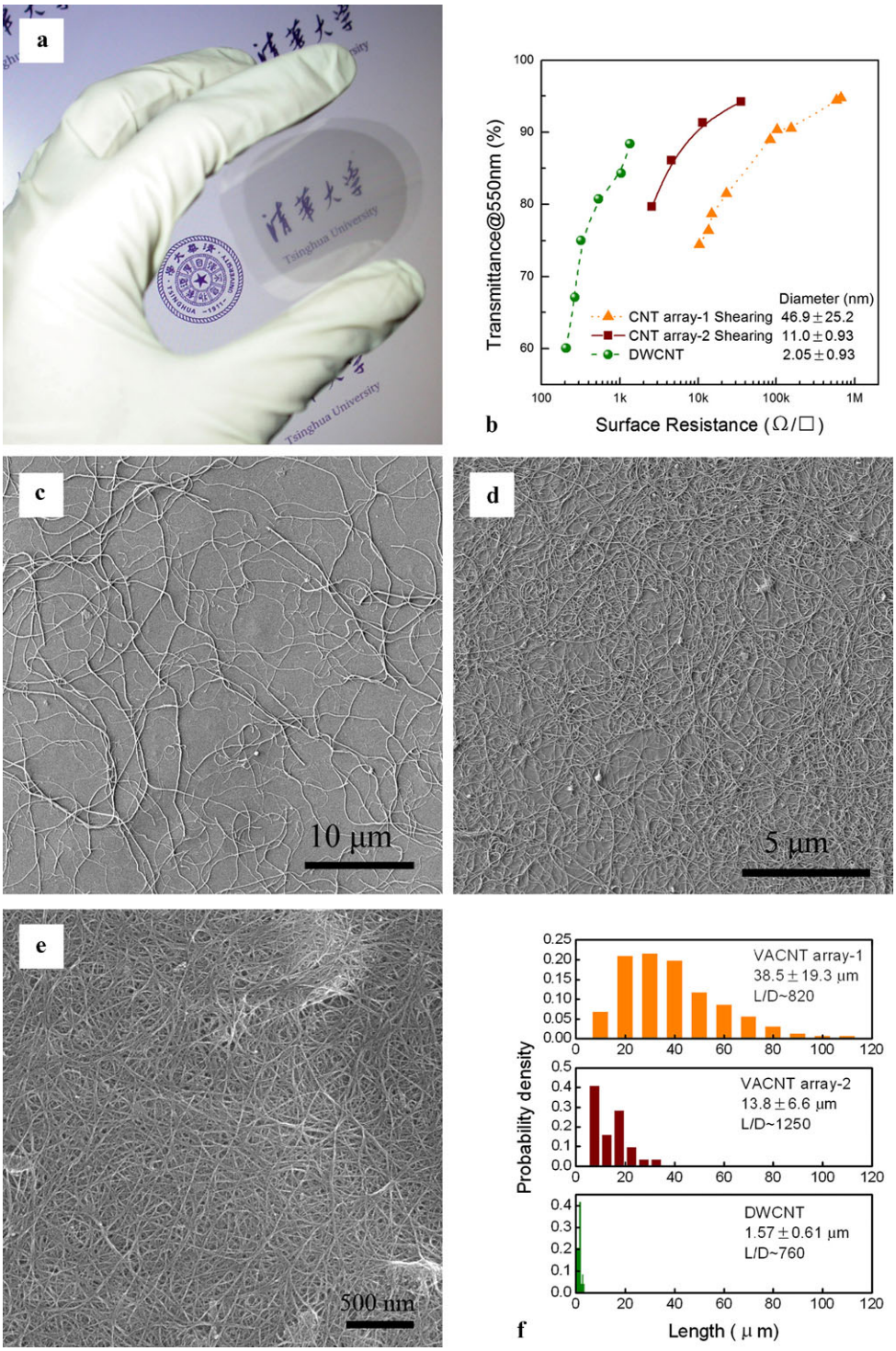

Fig. 2 (**a**) A typical photograph of a CNT TCF on a PET substrate; (**b**) the electro-optical properties of TCFs made from VACNT array-1, VACNT array-2, and DWCNTs; (**c**–**e**) SEM images of them, respectively; (**f**) the length distribution of the three kinds of CNTs

was 3.88. The reported σ_{dc}/σ_{op} ratios of DWCNTs were about 0.588–1.72 [24, 45, 50]. The σ_{dc}/σ_{op} ratio of sorted DWCNTs was 8.3 [50]. SWCNTs (~1.4 nm) obtained from the arc-discharge method always have a quite high σ_{dc}/σ_{op} ratio of over 10 [51–53].

The CNT diameter affected the σ_{dc}/σ_{op} ratio significantly. The relationship between σ_{dc}/σ_{op} ratio and CNT diameter is drawn in Fig. 3c. With the increasing of wall number, the diameter of the CNTs became larger, and the σ_{dc}/σ_{op} ratio was proportional to $1/D$ (when the diameter of the CNTs was larger than 1.4 nm), where D is the CNT diameter. It is well known that the conduction of electrons by MWCNTs mainly depends on the outmost layer [54]. The transmittance of MWCNTs was still deteriorated by ab-

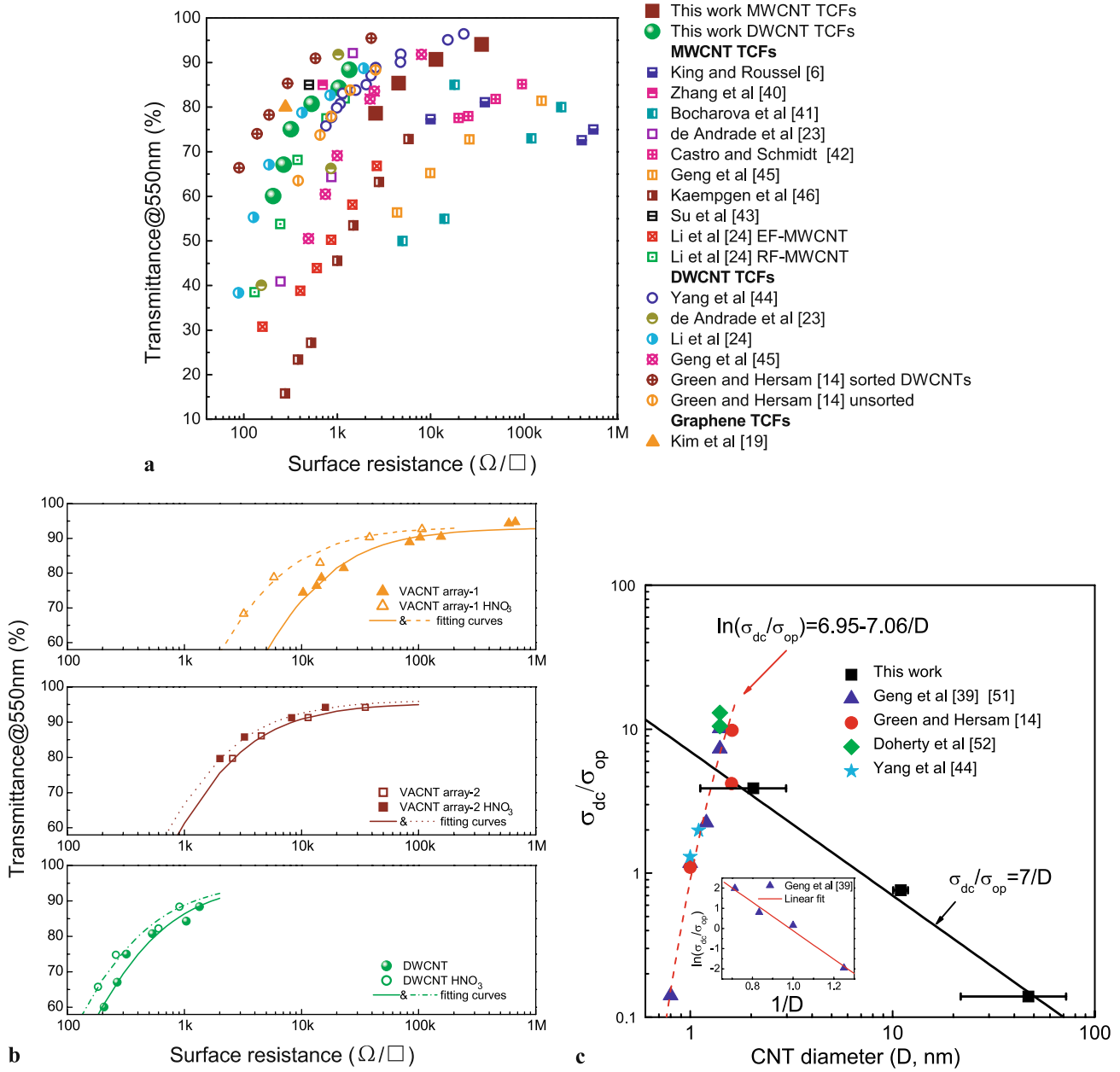

Fig. 3 (**a**) The electro-optical properties of TCFs from this work and from the literature using MWCNTs (*square points*), DWCNTs (*circle points*), and graphene (*triangle points*). (**b**) The electro-optical properties of TCFs from different kinds of CNTs before and after HNO_3 post-treatment. (**c**) The relationship between σ_{dc}/σ_{op} ratio and CNT diameter

sorption and Rayleigh scattering of the inner walls [47]. As the diameter decreased, the wall numbers usually decreased, the transmittance was enhanced, and thus the σ_{dc}/σ_{op} ratio increased. This indicated that the utilization efficiency of CNT walls was enhanced for small-diameter CNTs. However, the σ_{dc}/σ_{op} ratio increased as the SWCNT diameter increased (when the diameter of the SWCNTs was smaller than 1.4 nm). Since both the band gap of semi-conducting nanotubes and the pseudogap of metallic nanotubes were inversely proportional to the CNT diameter, and the conductivity decreases exponentially with band gap [39], the conductivity increased as the CNT diameter increased and led to the increase of the σ_{dc}/σ_{op} ratio. The inset image shows that $\ln(\sigma_{dc}/\sigma_{op})$ was proportional to $1/D$ using the data from Geng et al. [39].

To further improve the properties of TCFs, various approaches, such as immersion of SWCNT films in HNO_3 [11], $SOCl_2$ [55], and HNO_3 followed by $SOCl_2$ [56], and deposition of gold nanoparticles [44], have been explored to enhance the conductivities of TCFs. Here, HNO_3 treat-

Table 1 The fitting parameters of TCFs made from different kinds of CNTs, before and after HNO_3 post-treatment

CNTs	Preparation method	Diameter (D, nm)	Initial length (μm)	Initial L/D	Dispersion method	Length after dispersion (μm)	Average L/D after dispersion	Treatment of TCFs	t	$\frac{\sigma_{dc}}{\sigma_{op}}$
VACNT array-1	Floating catalyst CVD	46.9 ± 25.2	5000	$\sim 10^5$	Shearing	38.5 ± 19.3	~820	–	0.930	0.139
								HNO_3	0.935	0.338
VACNT array-2	Thermal CVD	11.0 ± 0.93	200	~18000	Shearing	13.8 ± 6.6	~1250	–	0.954	0.760
								HNO_3	0.963	0.939
DWCNT	Fe/MgO CVD	2.05 ± 0.93	~10	~4900	SDS sonication	1.57 ± 0.61	~760	–	0.955	3.88
								HNO_3	0.942	5.24

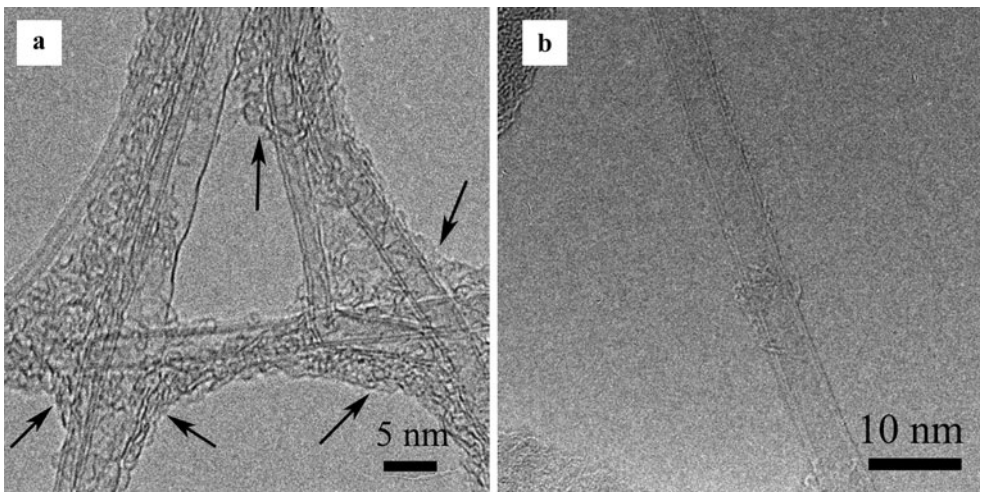

Fig. 4 HRTEM images of DWCNT TCFs (**a**) before and (**b**) after HNO_3 post-treatment

ment was adopted for both MWCNT and DWCNT TCFs for the reason that this can give a higher σ_{dc}/σ_{op} ratio [11, 51]. Geng et al. [11] reported that HNO_3 treatment was effective to reduce the surface resistance of SWCNT TCFs, and the effect of acid treatment is mainly to remove the SDS and enhance the metallicity of the films. In our case, all kinds of TCFs were treated by dipping into HNO_3 solution. In all cases, the surface resistance decreased while the transmittance did not change much (Fig. 3b). The performances of treated TCFs were 6.0 kΩ/□ at 78.2% T, 2.0 kΩ/□ at 79.5% T, and 260 Ω/□ at 74.8% T for TCFs from VACNT array-1, VACNT array-2, and DWCNTs, respectively. The fitting curves are shown in Fig. 3b, which fitted well with the experimental data, and the fitting parameters are shown in Table 1. The σ_{dc}/σ_{op} ratios increased to 0.338, 0.939, and 5.24, respectively. Compared with the SDS-dispersed SWCNTs [11], the VACNT arrays were dispersed without the assistance of surfactant and the MWCNTs in the array were metallic tubes. The σ_{dc} enhancement of MWCNT films after treatment by mixed acid has also been reported [57]. Picozzi et al. reported that the oxygen-containing functional groups introduced during acid treatment increased the number of bands near the Fermi level, promoting electron transfer between the carbon atoms [58]. This was regarded as the mechanism for the performance improvement for MWCNT TCFs.

For DWCNT TCFs, the surface was coated with a layer of SDS molecules before HNO_3 treatment, as illustrated by the black arrows in Fig. 4a. The insulating SDS molecule will degrade the conductivity of the TCFs. After HNO_3 treatment, the surface of DWCNTs was clean and no surfactant molecules were found (Fig. 4b). The results were in good accordance with those observed for the SWCNT TCFs [51].

To further investigate the effect of HNO_3 treatment, the surface resistance and Raman spectra of a thick DWCNT film were recorded after different treatment times (Fig. 5). The surface resistance reduced sharply to about 1/10 of the original value after a 10-min treatment. Then the surface resistance kept stable with longer treatment (180 min). The tendency was in agreement with that reported for SWCNT TCFs [11]. Meanwhile, the film thickness decreased from 18.2 to 10.6 μm, and the ratio of the Raman intensities of the D-peak to the G-peak (I_D/I_G) increased from 0.16 to 0.3 after a 10-min treatment. The film thickness and

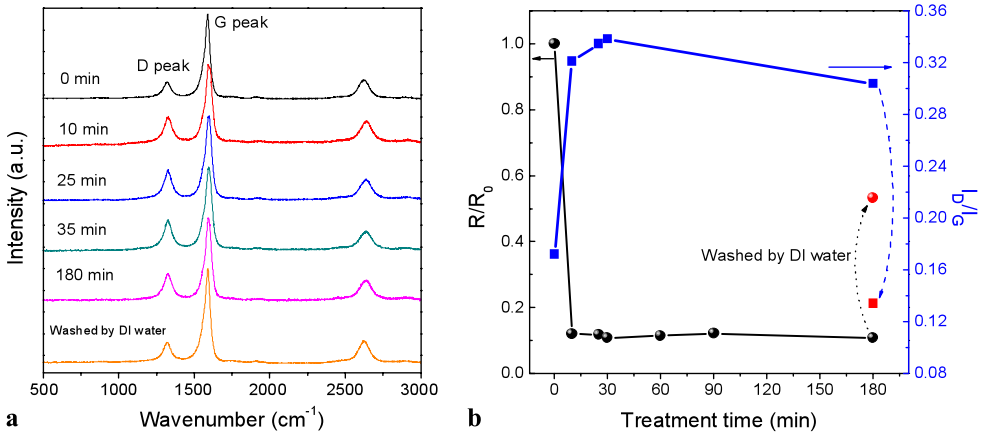

Fig. 5 (**a**) Raman spectra and (**b**) relative resistance and I_D/I_G ratio of DWCNT TCFs before treatment, after immersion in HNO_3 solution for different periods of time, and after washing by de-ionized water

I_D/I_G ratio both reached a plateau after longer treatment. It was assumed that oxygen, as an electron acceptor, exhibiting higher electron negativity is physisorbed on the pristine DWCNTs after HNO_3 treatment, which also resulted in an increase of the I_D/I_G ratio [59]. The decrease of the surface resistance was attributed to the increase of the hole concentration from specific bands due to doping with electron acceptors such as oxygen [44]. Conclusively, due to the removal of SDS molecules, the reduction of the film thickness, and likely the doping with electron acceptors such as oxygen, the surface resistance after HNO_3 treatment decreased.

The film was further washed by de-ionized water repeatedly to thoroughly remove the HNO_3. After that, the resistance changed from 1/10 to about half of the original value. The I_D/I_G ratio even decreased to 0.13 after washing while the film thickness did not change obviously. The removal of amorphous carbon at the CNT surface after HNO_3 treatment was considered as the main reason for the decrease of the I_D/I_G ratio. The surface resistance was still half of the original value, which was due to removal of SDS molecules and the reduction of the film thickness produced by HNO_3 treatment.

4 Conclusions

In conclusion, DWCNTs and two kinds of vertically aligned MWCNTs were used as raw materials to fabricate TCFs. The performances of TCFs made from VACNT array-2 and DWCNTs were superior to most results in the literature due to the long length and high aspect ratio of the as-dispersed CNTs. DWCNTs constructed the densest conductive network at the same transmittance and the corresponding TCFs showed the best performance (320 Ω/□ at 75.0% T). The σ_{dc}/σ_{op} ratios of the three TCFs were 0.139, 0.76, and 3.88, respectively. The TCFs were treated by HNO_3 to reduce the surface resistance. The decrease of surface resistance after HNO_3 treatment was attributed to the removal of SDS molecules, the reduction of the film thickness and likely the doping with electron acceptors such as oxygen. The σ_{dc}/σ_{op} ratio of the DWCNTs was increased to 5.24, which was comparable with that of arc-discharge SWCNTs. The as-obtained D/MWCNT TCFs were promising for applications such as flat-panel displays, organic light-emitting diodes, solar cells, etc.

Acknowledgements This study was supported by the Foundation for the Natural Scientific Foundation of China (Nos. 20736004, 20736007, and 2007AA03Z346) and the China National Program (No. 2006CB932702).

References

1. G. Gruner, J. Mater. Chem. **16**, 3533 (2006)
2. Q. Cao, J.A. Rogers, Nano Res. **1**, 259 (2008)
3. Q. Cao, J.A. Rogers, Adv. Mater. **21**, 29 (2009)
4. H.W. Zhu, J.Q. Wei, K.L. Wang, D.H. Wu, Sol. Energy Mater. Sol. Cells **93**, 1461 (2009)
5. H. Gu, T.M. Swager, Adv. Mater. **20**, 4433 (2008)
6. R.C.Y. King, F. Roussel, Appl. Phys. A **86**, 159 (2007)
7. D.H. Zhang, K. Ryu, X.L. Liu, E. Polikarpov, J. Ly, M.E. Tompson, C.W. Zhou, Nano Lett. **6**, 1880 (2006)
8. Y. Wang, C.A. Di, Y.Q. Liu, H. Kajiura, S.H. Ye, L.C. Cao, D.C. Wei, H.L. Zhang, Y.M. Li, K. Noda, Adv. Mater. **20**, 4442 (2008)
9. S.F. Pei, J.H. Du, Y. Zeng, C. Liu, H.M. Cheng, Nanotechnology **20**, 235707 (2009)
10. A.A. Green, M.C. Hersam, Nano Lett. **8**, 1417 (2008)
11. H.Z. Geng, K.K. Kim, K.P. So, Y.S. Lee, Y. Chang, Y.H. Lee, J. Am. Chem. Soc. **129**, 7758 (2007)
12. Y. Wang, L.P. Huang, Y.Q. Liu, D.C. Wei, H.L. Zhang, H. Kajiura, Y.M. Li, Nano Res. **2**, 865 (2009)
13. W.Q. Fu, L. Liu, K.L. Jiang, Q.Q. Li, S.S. Fan, Carbon **48**, 1876 (2010)
14. A.A. Green, M.C. Hersam, Nat. Nanotechnol. **4**, 64 (2009)
15. T. Kitano, Y. Maeda, T. Akasaka, Carbon **47**, 3559 (2009)
16. S. Paul, D.W. Kim, Carbon **47**, 2436 (2009)
17. J.Q. Wei, Y. Jia, Q.K. Shu, Z.Y. Gu, K.L. Wang, D.M. Zhuang, G. Zhang, Z.C. Wang, J.B. Luo, A.Y. Cao, D.H. Wu, Nano Lett. **7**, 2317 (2007)
18. S. De, J.N. Coleman, ACS Nano **4**, 2713 (2010)
19. K.S. Kim, Y. Zhao, H. Jang, S.Y. Lee, J.M. Kim, K.S. Kim, J.H. Ahn, P. Kim, J.Y. Choi, B.H. Hong, Nature **457**, 706 (2009)

20. Y.P. Wu, B. Wang, Y.F. Ma, Y. Huang, N. Li, F. Zhang, Y.S. Chen, Nano Res. **3**, 661 (2010)
21. N. Saran, K. Parikh, D.S. Suh, E. Munoz, H. Kolla, S.K. Manohar, J. Am. Chem. Soc. **126**, 4462 (2004)
22. B. Dan, G.C. Irvin, M. Pasquali, ACS Nano **3**, 835 (2009)
23. M.J. de Andrade, M.D. Lima, V. Skakalova, C.P. Bergmann, S. Roth, Phys. Status Solidi RRL **1**, 178 (2007)
24. Z.R. Li, H.R. Kandel, E. Dervishi, V. Saini, Y. Xu, A.R. Biris, D. Lupu, G.J. Salamo, A.S. Biris, Langmuir **24**, 2655 (2008)
25. Z.R. Li, H.R. Kandel, E. Dervishi, V. Saini, A.S. Biris, A.R. Biris, D. Lupu, Appl. Phys. Lett. **91**, 053115 (2007)
26. D. Simien, J.A. Fagan, W. Luo, J.F. Douglas, K. Migler, J. Obrzut, ACS Nano **2**, 1879 (2008)
27. A.N.G. Parra-Vasquez, I. Stepanek, V.A. Davis, V.C. Moore, E.H. Haroz, J. Shaver, R.H. Hauge, R.E. Smalley, M. Pasquali, Macromolecules **40**, 4043 (2007)
28. A. Kaskela, A.G. Nasibulin, M.Y. Timmermans, B. Aitchison, A. Papadimitratos, Y. Tian, Z. Zhu, H. Jiang, D.P. Brown, A. Zakhidov, E.I. Kauppinen, Nano Lett. **10**, 4349 (2010)
29. Q. Zhang, G.H. Xu, J.Q. Huang, W.P. Zhou, M.Q. Zhao, Y. Wang, W.Z. Qian, F. Wei, Carbon **47**, 538 (2009)
30. H. Sugime, S. Noda, Carbon **48**, 2203 (2010)
31. J.Q. Huang, Q. Zhang, F. Wei, W.Z. Qian, D.Z. Wang, L. Hu, Carbon **46**, 291 (2008)
32. Q. Zhang, J.Q. Huang, M.Q. Zhao, W.Z. Qian, Y. Wang, F. Wei, Carbon **46**, 1152 (2008)
33. Q. Zhang, M.Q. Zhao, Y. Liu, A.Y. Cao, W.Z. Qian, Y.F. Lu, F. Wei, Adv. Mater. **21**, 2876 (2009)
34. Q. Zhang, M.Q. Zhao, J.Q. Huang, Y. Liu, Y. Wang, W.Z. Qian, F. Wei, Carbon **47**, 2600 (2009)
35. Y. Liu, W.Z. Qian, Q. Zhang, G.Q. Ning, G.H. Luo, Y. Wang, D.Z. Wang, F. Wei, Chem. Eng. Technol. **32**, 73 (2009)
36. X.B. Zhang, K.L. Jiang, C. Teng, P. Liu, L. Zhang, J. Kong, T.H. Zhang, Q.Q. Li, S.S. Fan, Adv. Mater. **18**, 1505 (2006)
37. G.H. Xu, Q. Zhang, J.Q. Huang, M.Q. Zhao, W.P. Zhou, F. Wei, Langmuir **26**, 2798 (2010)
38. Z.C. Wu, Z.H. Chen, X. Du, J.M. Logan, J. Sippel, M. Nikolou, K. Kamaras, J.R. Reynolds, D.B. Tanner, A.F. Hebard, A.G. Rinzler, Science **305**, 1273 (2004)
39. H.Z. Geng, K.K. Kim, K. Lee, G.Y. Kim, H.K. Choi, D.S. Lee, K.H. An, Y.H. Lee, Y. Chang, Y.S. Lee, B. Kim, Y.J. Lee, Nano **2**, 157 (2007)
40. M. Zhang, S.L. Fang, A.A. Zakhidov, S.B. Lee, A.E. Aliev, C.D. Williams, K.R. Atkinson, R.H. Baughman, Science **309**, 1215 (2005)
41. V. Bocharova, A. Kiriy, U. Oertel, M. Stamm, F. Stoffelbach, R. Jerome, C. Detrembleur, J. Phys. Chem. B **110**, 14640 (2006)
42. M.R.S. Castro, H.K. Schmidt, Mater. Chem. Phys. **111**, 317 (2008)
43. J.W. Su, S.J. Fu, S. Gwo, K.J. Lin, Chem. Commun. 5631 (2008)
44. S.B. Yang, B.S. Kong, J. Geng, H.T. Jung, J. Phys. Chem. C **113**, 13658 (2009)
45. H.Z. Geng, D.S. Lee, K.K. Kim, S.J. Kim, J.J. Bae, Y.H. Lee, J. Korean Phys. Soc. 979 (2008)
46. M. Kaempgen, G.S. Duesberg, S. Roth, Appl. Surf. Sci. **252**, 425 (2005)
47. J.T. Han, S.Y. Kim, J.S. Woo, G.W. Lee, Adv. Mater. **20**, 3724 (2008)
48. L. Hu, D.S. Hecht, G. Gruner, Nano Lett. **4**, 2513 (2004)
49. Y.X. Zhou, L.B. Hu, G. Gruner, Appl. Phys. Lett. **88**, 123109 (2006)
50. P.N. Nirmalraj, P.E. Lyons, S. De, J.N. Coleman, J.J. Boland, Nano Lett. **9**, 3890 (2009)
51. H.Z. Geng, D.S. Lee, K.K. Kim, G.H. Han, H.K. Park, Y.H. Lee, Chem. Phys. Lett. **455**, 275 (2008)
52. E.M. Doherty, S. De, P.E. Lyons, A. Shmeliov, P.N. Nirmalraj, V. Scardaci, J. Joimel, W.J. Blau, J.J. Boland, J.N. Coleman, Carbon **47**, 2466 (2009)
53. S. De, P.E. Lyons, S. Sorel, E.M. Doherty, P.J. King, W.J. Blau, P.N. Nirmalraj, J.J. Boland, V. Scardaci, J. Joimel, J.N. Coleman, ACS Nano **3**, 714 (2009)
54. C. Berger, Y. Yi, J. Gezo, P. Poncharal, W.A. de Heer, New J. Phys. **5**, 16 (2003)
55. U. Dettlaff-Weglikowska, V. Skakalova, R. Graupner, S.H. Jhang, B.H. Kim, H.J. Lee, L. Ley, Y.W. Park, S. Berber, D. Tomanek, S. Roth, J. Am. Chem. Soc. **127**, 5125 (2005)
56. B.B. Parekh, G. Fanchini, G. Eda, M. Chhowalla, Appl. Phys. Lett. **90**, 121913 (2007)
57. G.H. Xu, Q. Zhang, W.P. Zhou, J.Q. Huang, F. Wei, Appl. Phys. A **92**, 531 (2008)
58. S. Picozzi, S. Santucci, L. Lozzi, C. Cantalini, C. Baratto, G. Sberveglieri, I. Armentano, J.M. Kenny, L. Valentini, B. Delley, J. Vac. Sci. Technol. A **22**, 1466 (2004)
59. M. Kaempgen, M. Lebert, M. Haluska, N. Nicoloso, S. Roth, Adv. Mater. **20**, 616 (2008)